ADVANCES IN ATMOSPHERIC SCIENCES, VOL. 24, NO. 1, 2007, 35–43

Roles of Mesoscale Terrain and Latent Heat Release in Typhoon Precipitation: A Numerical Case Study

LI Yunying*[1,2] (李昀英), HUANG Wei[3] (黄 伟), and ZHAO Jiaozhi[4] (赵焦枝)

[1]*State Key Laboratory of Numerical Modeling for Atmospheric Sciences and Geophysical Fluid Dynamics, Institute of Atmospheric Physics, Chinese Academy of Sciences, Beijing* 100029

[2]*Institute of Meteorology, PLA University of Science and Technology, Nanjing* 211101

[3]*Shanghai Typhoon Institute, China Meteorological Administration, Shanghai* 200030

[4]*Meteorology Center of Beijing Military, PLAAF, Beijing* 100061

(Received 8 November 2005; revised 6 June 2006)

ABSTRACT

The mesoscale orographic effects on typhoon Aere's precipitation are simulated using an Advanced Regional Eta-coordinate Model (AREM) version 3.0. In particular, the effects of the latent heat release are studied by two comparable experiments: with and without condensational heating. The results show that the typhoon rainfall is tripled by the southeastern China mesoscale terrain, and the condensational heating is responsible for at least half of the increase. One role of the latent heat release is to warm the atmosphere, leading to a depression of the surface pressure, which then causes a larger pressure difference in the zonal direction. This pressure gradient guides the water vapour to flow into the foothills, which in turn amplifies the water vapour flux divergence amplified, causing the typhoon rainfall to increase eventually. The other role of the latent heat release is to make the convection more organized, resulting in a relatively smaller rain area and stronger precipitation.

Key words: latent heat release, mesoscale terrain, typhoon precipitation, numerical modeling

DOI: 10.1007/s00376-007-0035-8

1. Introduction

There is little doubt that the mountains profoundly affect the formation and development of rain systems (Smith, 1979; Tao, 1980; Carbone et al., 1995; Buzzi et al., 1998; Kodama and Barnes, 1997; Neiman et al., 2002; Zang et al., 2004), especially in mountainous countries like China. Typhoon rainstorms, one of the originators of flooding in China, are often greatly influenced by the mesoscale terrain. In general, tropical storms affecting China may form in the West Pacific Ocean or South China Sea, which then move northwestward under internal and external forces. When typhoons land at China's Zhejiang, Fujian, or Guangdong provinces, they will hit mesoscale mountains such as Wufeng Mountain (mean elevation of about 800 m) and Daiyun Mountain (mean elevation of about 600 m), which are orientated in a NE-SW direction and are parallel to the coastline (Fig. 1a). The prevailing winds associated with typhoons usually cross the mountains from the east, and statistically cause an increase in rainfall. Some previous works (Pauley and Smith, 1988; Fosdick and Smith, 1991; Liu et al., 2001; Posselt and Martin, 2004) have indicated that the latent heat release (LHR) could change the basic structures of the synoptic systems, and may play a key role in the rainfall increase (Brennan and Lackmann, 2005). But to what extent, and how LHR and typhoon precipitation interact with each other under mesoscale orographic effects are so far unclear. Since the influences of the terrain and LHR are often mixed with other factors and cannot be easily separated by the observational data, using high resolution numerical experiments to study the effect of LHR under mesoscale orographic effects would significantly help our understanding and improve typhoon rainfall forecasting (Gao et al., 1994; Zhai et al., 1995; Zhou and Qian, 1996; Feng et al., 2004).

*E-mail: liyunying2005@163.com

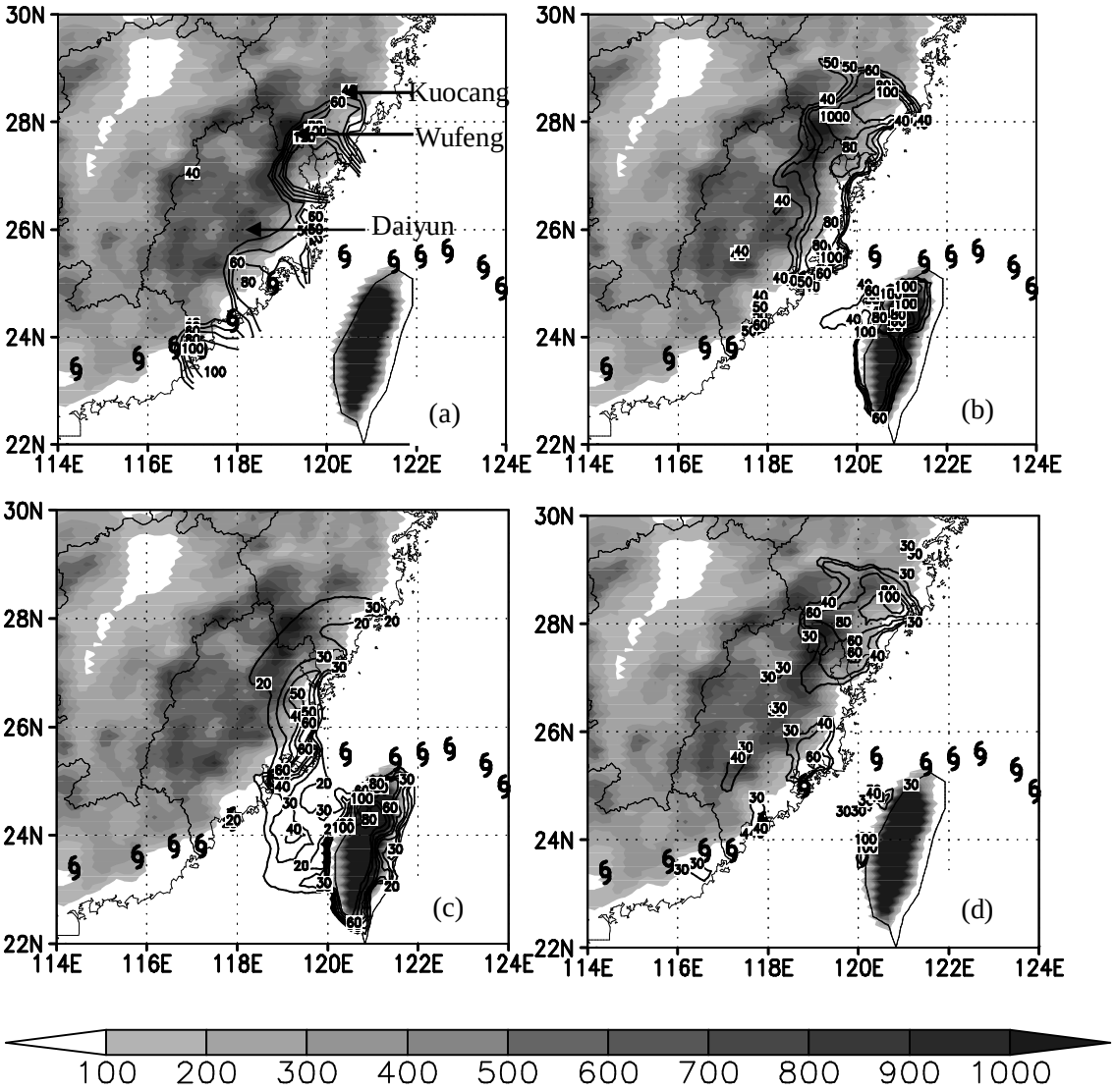

Fig. 1. Total rainfall (mm) from 0000 UTC 25 to 0000 UTC 26 August 2004 derived from (a) observation, (b) EXP_CTL and (c) EXP_noterrain. (d) The rainfall difference between EXP_CTL and EXP_noterrain. Terrain heights (m) in the AREM model are shaded according to the legend. The observed path of typhoon Aere is marked by typhoon symbols. Red stands for typhoon and yellow stands for tropical storm.

Typhoon Aere, the 18th one to occur in 2004 and second most powerful typhoon to sweep China, formed in the eastern Philippine Sea on 19 August 2004, moved northwestward and landed at Fuqing city at 0830 UTC 25 August. Then, guided by the northeast wind around the southeast side of the subtropical high pressure, it ran southwestward along the coastline, moved into Guangdong province and downgraded to a tropical storm at 0600 UTC 26 August (the path is shown with typhoon markers in Fig. 1). Under the influence of typhoon Aere, flash floods occurred. From 0000 UTC 25 to 0000 UTC 26 August, Aere produced more than 50 mm of precipitation at 22 observational stations, 100 mm at 8 stations, and 200 mm at 3 stations in Fujian province. Zherong county (27.15°N, 119.54°E, 670.0 m), with a relatively higher elevation in this area, and being the entrance of the water vapour inflows connected to a strong spiral cloud band outside the typhoon eye, received the maximum rainfall of 407 mm in 24 h. The black isolines in Fig. 1a illustrate the observed rainfall from 0000 UTC 25 August to 0000 UTC 26 August. The heavy rain center appeared on the east side of the Wufeng Mountain peak (ESWM), the 50 mm isoline of rainfall was approximately parallel to the mountain's orientation, indicating the terrain's possible role in the flood event. In this paper, based on the numerical simulations, we take Aere as a case to examine the mesoscale terrain

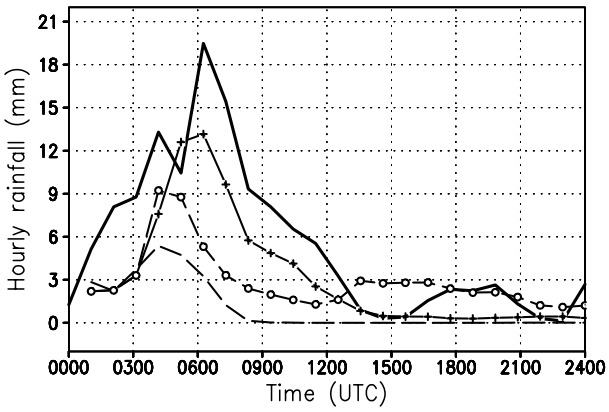

Fig. 2. Hourly rainfall (mm h^{-1}) averaged in the region (27°–28°N, 120°–121°E) derived from observations (solid line), EXP_CTL (solid line with +), EXP_noheat (dashed line with o), and EXP_noterrain (dashed line).

effects on the typhoon rainstorm and to study the role of LHR. The organization of this paper is as follows: section 2 is a brief description of the AREM model (Advanced Regional Eta-coordinate Model, Yu and Xu, 2004), section 3 examines the mesoscale orographic effects on the rainstorm, the role of LHR is studied in section 4, and section 5 contains some conclusions and discussions.

2. Model description

AREM is a regional Eta-coordinate, hydrostatic weather forecasting model. A 10′ resolution terrain is used and treated as three-dimensional steps in the model to decrease the errors of pressure gradient over the mountainous areas. The model domain covers 0°–70°N, 50°–150°E with a 12 km×12 km horizontal resolution and 32 uneven levels in the vertical from the surface to 10 hPa. A two-step shape-preserving advection scheme (Yu, 1994) is used to keep a reasonable moisture advection in the model dynamical core. The AREM model has now been developed to version 3.0 and is widely used in research and operational forecasting in China and other Asian countries, and it is proved to have a distinct advantage in precipitation forecasting.

The model physical processes used in this work include the explicit prognostic warm cloud scheme (Xu et al., 1998), the modified Betts convective adjustment scheme (1986), a non-local diffusion boundary layer parameterization scheme (Holtslag and Boville, 1993), a surface flux calculation by a whole exchange coefficient method (Deardorff, 1972) and a radiation parameterization (Benjamin and Seaman, 1985). The model runs in the domain 15°–40°N, 100°–130°E under fixed boundary conditions, and is integrated from 0000 UTC 25 August to 0000 UTC 26 August, 2004, using the NCEP (National Centers for Environmental Prediction) 1° × 1° objective analysis data as the initial fields.

3. Rainfall increased by mesoscale terrain

Aere moved southeastward after landing in Fujian province, and an associated rain belt appeared on the east side of the Wufeng and Daiyun mountains. Figure 1b illustrates the simulated precipitation from 0000 UTC 25 August to 0000 UTC 26 August in the control run (called EXP_CTL). The rain belt parallels the orientation of Wufeng and Daiyun mountains, and the center stays in the ESWM with the maximum of 124 mm, in accordance with the observations. However, another center with a larger rainfall than the observation forms in the valley between Wufeng Mountain and Kuocang Mountain (hence called the Wu-Kuo valley). We find a simulated 0.5° north bias in the typhoon landing spot (figure omitted) and the blocking effect of the Wu-Kuo valley might be responsible for this unrealistic precipitation center.

When the terrain heights are set to zero in the initial fields (called EXP_noterrain), the total rainfall is much smaller in the ESWM (the maximum is only 40 mm), and the center also drifts to the south (Fig. 1c). The result reveals that the precipitation in the ESWM may be triggered by the upward motion within the typhoon spiral cloud band rather than by the terrain, but the mesoscale mountains increase the rainfall seriously. The rainfall difference between EXP_CTL and EXP_noterrain is shown as Fig. 1d. The maximal difference occurs in the Wu-Kuo valley, another difference center appears in the ESWM, with the maximum value of 80 mm, and the 30 mm isoline of the rainfall difference parallels the mountain orientation. This sensitivity experiment shows that the maximum precipitation is tripled by mesoscale mountains, and the rainfall peak also rises from 5 mm h^{-1} to 13 mm h^{-1} (Fig. 2).

4. The role of latent heat release

The experiment EXP_noterrain shows that the precipitation increase is huge even though the mountain peak is lower than 1200 m. Does LHR act in this increase, and how? To answer this question, only LHR is removed from the diabatic term from the 4th to 10th hour of integration, which is the main rain period (this experiment is called EXP_noheat). Figures 3a to c illustrate the hourly precipitation at 0600–0700, 0700–

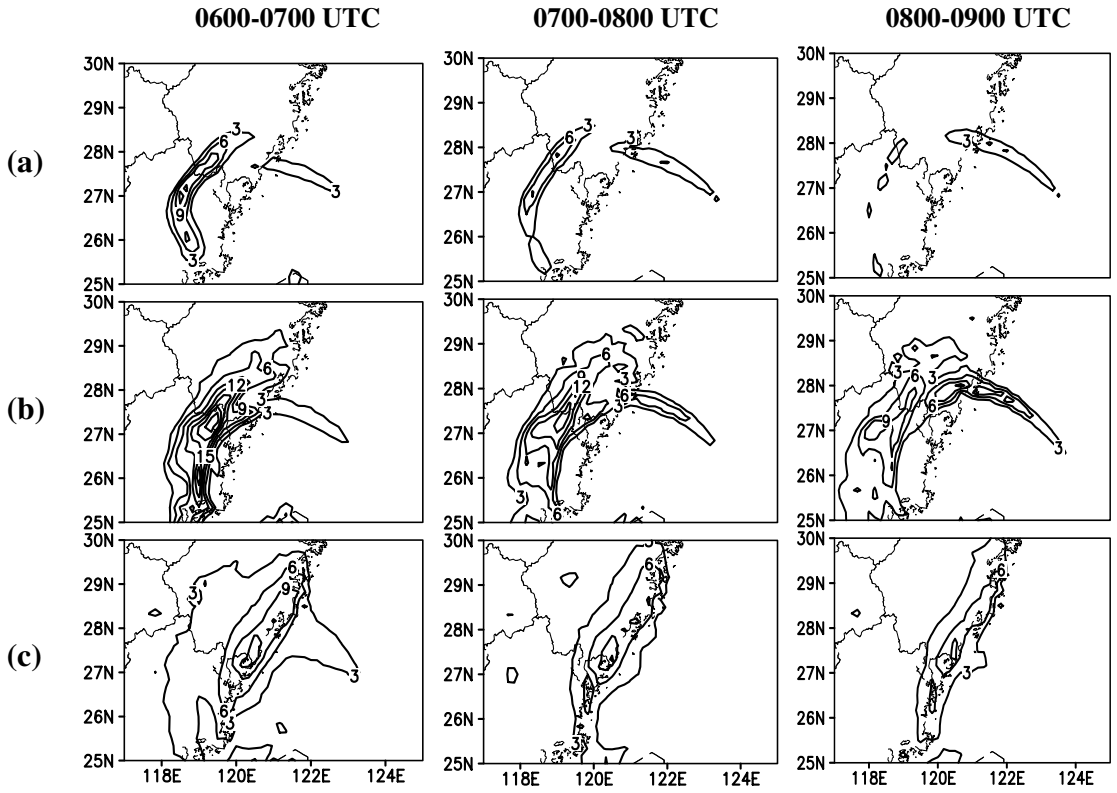

Fig. 3. Hourly precipitation (mm h^{-1}) in 0600–0700, 0700–0800, and 0800–0900 UTC simulated by (a) EXP_noterrain, (b) EXP_CTL, and (c) EXP_noheat.

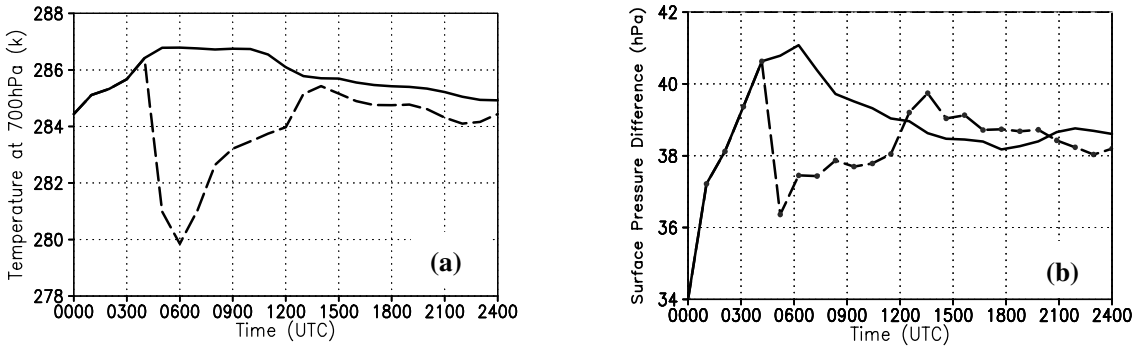

Fig. 4. (a) Hourly temperature (K) at 700 hPa, and (b) surface pressure difference (hPa) between the grid points (27.5°N, 122°E) and (27.5°N, 120°E) averaged over the region (27°–28°N, 119°–120°E) simulated by EXP_CTL (solid line) and EXP_noheat (dashed line).

0800 and 0800–0900 UTC in the different experiments. We find the maximum precipitation rate in the ESWM occurs at the moment that the water vapor transport band arrives at the foothills. The accompanying easterlies climb up along the mountain slopes, carry the water vapour to higher levels, and lead to rain. With zero terrain height, a relatively weaker spiral rain band exists in the East China Sea, but it has no link with the rain belt on the land (Fig. 3a). However, with the terrain forcing, the water vapour transport is strengthened, and a bridge between the rain belts over the sea and those over the land is established, or a passage of water vapour transport is built (Fig. 3b), and both rain belts on the land and on the sea are active. However, if the LHR is removed, the spiral rain band disappears gradually with time, so does the water vapour bridge (Fig. 3c). It seems that the mesoscale terrain forcing is an external factor in the precipitation increase, while

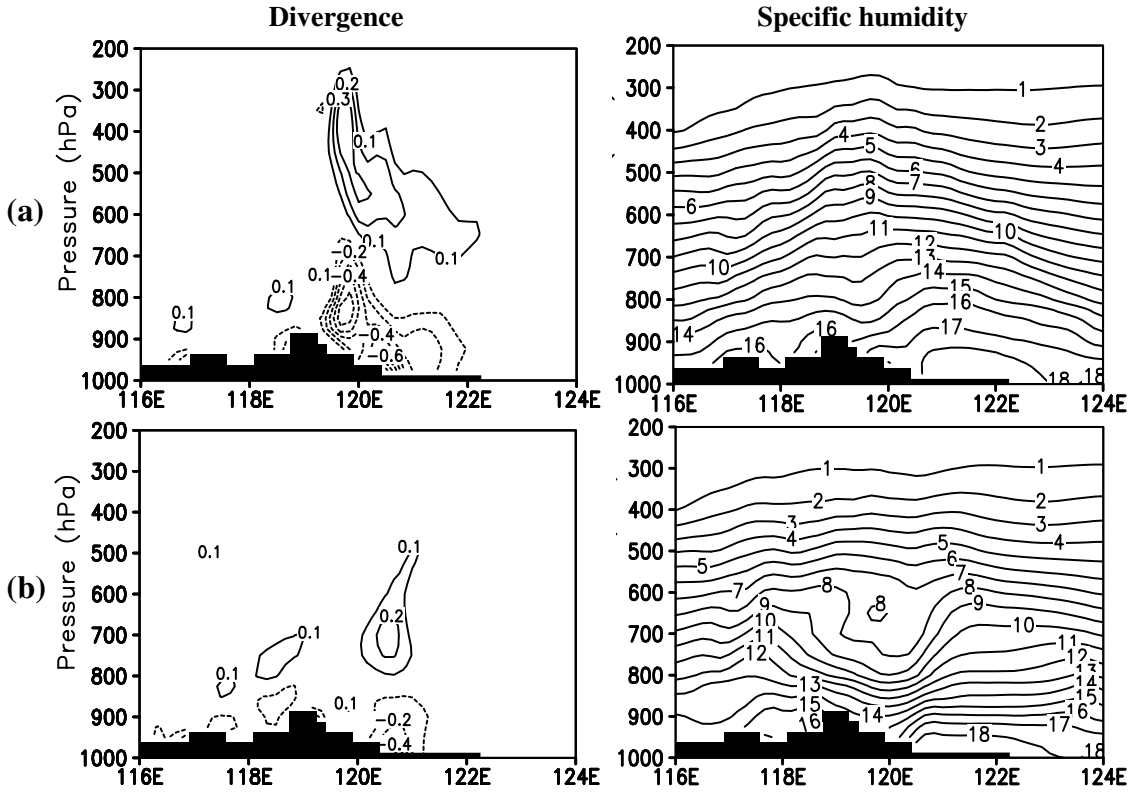

Fig. 5. Pressure-longitude cross sections of divergence (10^3 s^{-1}) and specific humidity (g kg^{-1}) along 27.5°N at 0700 UTC on 25 August simulated by (a) EXP_CTL and (b) EXP_noheat.

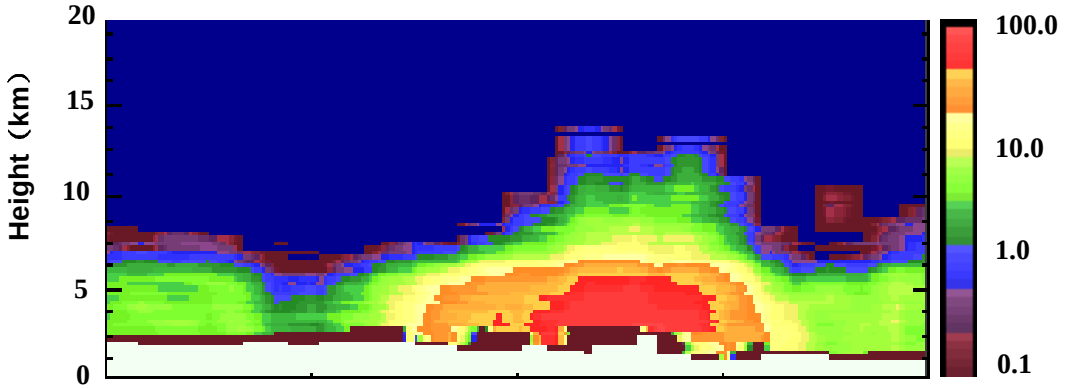

Fig. 6. Height-longitude cross section of precipitation rate (mm h^{-1}) along 28°N at 0731 UTC 25 August retrieved by TRMM PR.

LHR is an internal factor. With the LHR, how is this bridge constructed? Figure 4 may offer an explanation. Figures 4a and b illustrate the change of temperature and surface pressure with time at 700 hPa derived from EXP_CTL and EXP_noheat. Warmed by the latent heat release, the temperature in the middle troposphere becomes higher (the solid line in Fig. 4a), leading to a lower surface pressure and thus an increase of the pressure difference between the source region (the east part of the spiral water vapour band) and sink region (the west part of the spiral water vapour band) (the solid line in Fig. 4b). Then pressure gradient may guide the water vapour to move to the foothills, providing moisture for precipitation. When the water vapour band associated with the typhoon moves away, the water vapour supply may be cut off, and the rain stops gradually. When LHR is removed in the 4th integration hour, the temperature goes down

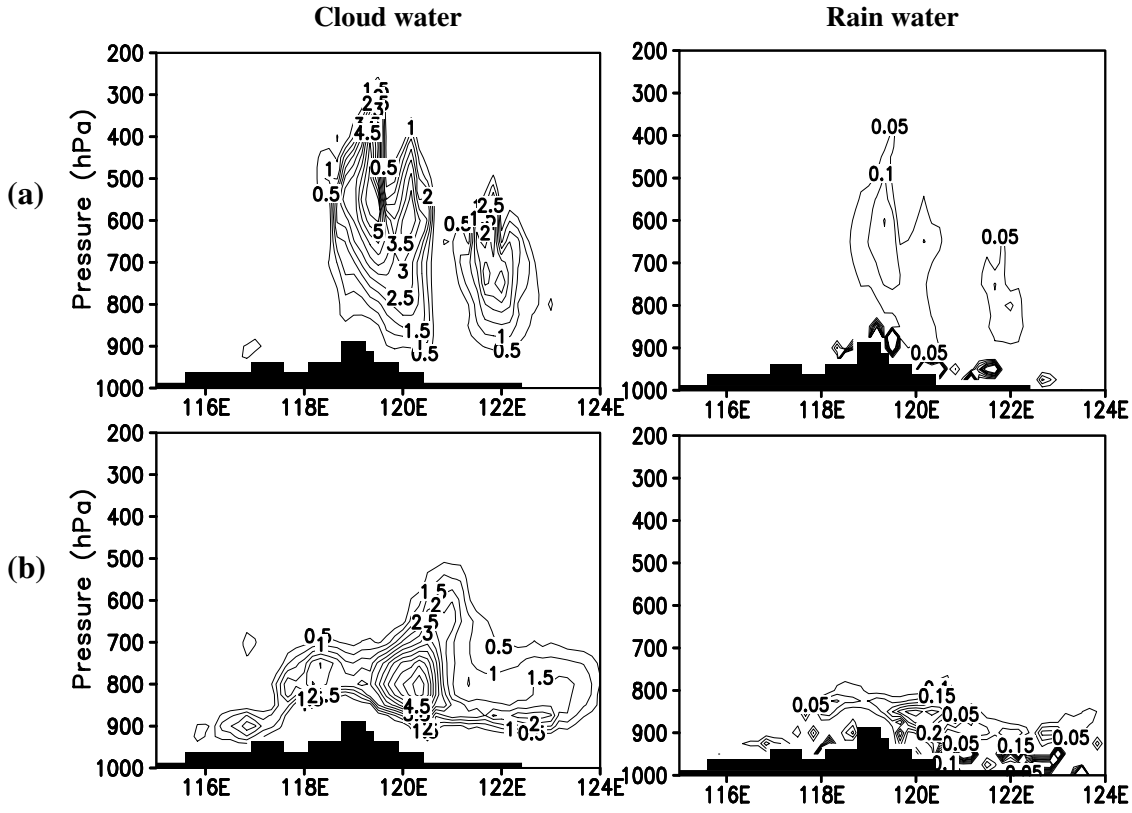

Fig. 7. Pressure-longitude cross sections of cloud water and rain water (g kg^{-1}) along 27.5°N at 0700 UTC 25 August simulated by (a) EXP_CTL and (b) EXP_noheat.

rapidly (see the dashed line in Fig. 4a), and the surface pressure difference decreases sharply (see the dashed line in Fig. 4b). Meanwhile, the water vapour transport band weakens or even disappears (see Fig. 3c). Then we could say one role of the LHR is to warm the air, thereby strengthening the ascending motion and water vapour transport.

With the stronger ascending motions, some elements such as divergence, vertical velocity and humidity are larger. Figures 5a and b are vertical distributions of divergence and specific humidity at 0700 UTC along 27.5°N in EXP_CTL and EXP_noheat, respectively. In EXP_CTL, the maximum values of the convergence and divergence are more than twice as large as those in EXP_noheat, and the divergence center occurs at a much higher level. Meanwhile, the water vapour can be transported to a relatively higher altitude. But in EXP_noheat, the water vapour piles up below 800 hPa and cannot be easily transported to the middle levels, forming a water vapour trough in the middle troposphere. All of the above evidence convinces us that LHR may enhance convection, lifting the air to higher levels.

Compared with EXP_noheat, the maximums of cloud water and rain rate can also occur at higher levels in EXP_CTL, similar to the observations. Figure 6 is the vertical distribution of the precipitation rate along 28°N retrieved by the TRMM (Tropical Rainfall Measuring Mission) PR (Precipitation Radar). Although the latitude (28°N) and the time (0731 UTC) of the radar scan are a little different from the precipitation center (27.5°N) and the maximum rainfall time (0600–0700 UTC), Fig. 6 should be able to reflect the basic features of the precipitation rate. The maximum precipitation rate occurs at height of 4 km, with the magnitude larger than 50 mm h^{-1}. Near the surface (about 2 km), the precipitation rate decreases to 0.1 mm h^{-1} though the returning echo is interfered with below 2 km. The corresponding distributions of the cloud water and rain water at 0700 UTC along 27.5°N derived from EXP_CTL and EXP_noheat are illustrated in Figs. 7a and b. The maximum cloud water appears at 600 hPa, and the top of the rain water is a little lower than that of cloud water in EXP_CTL. The cloud and rain water are mainly concentrated in two regions, exhibiting a smaller area and the features of convective rain. However, in EXP_noheat, the maximum cloud water appears at 800 hPa, and the rain water occurs at a much lower level. Meanwhile, the cloud and rain water have relatively homogeneous di-

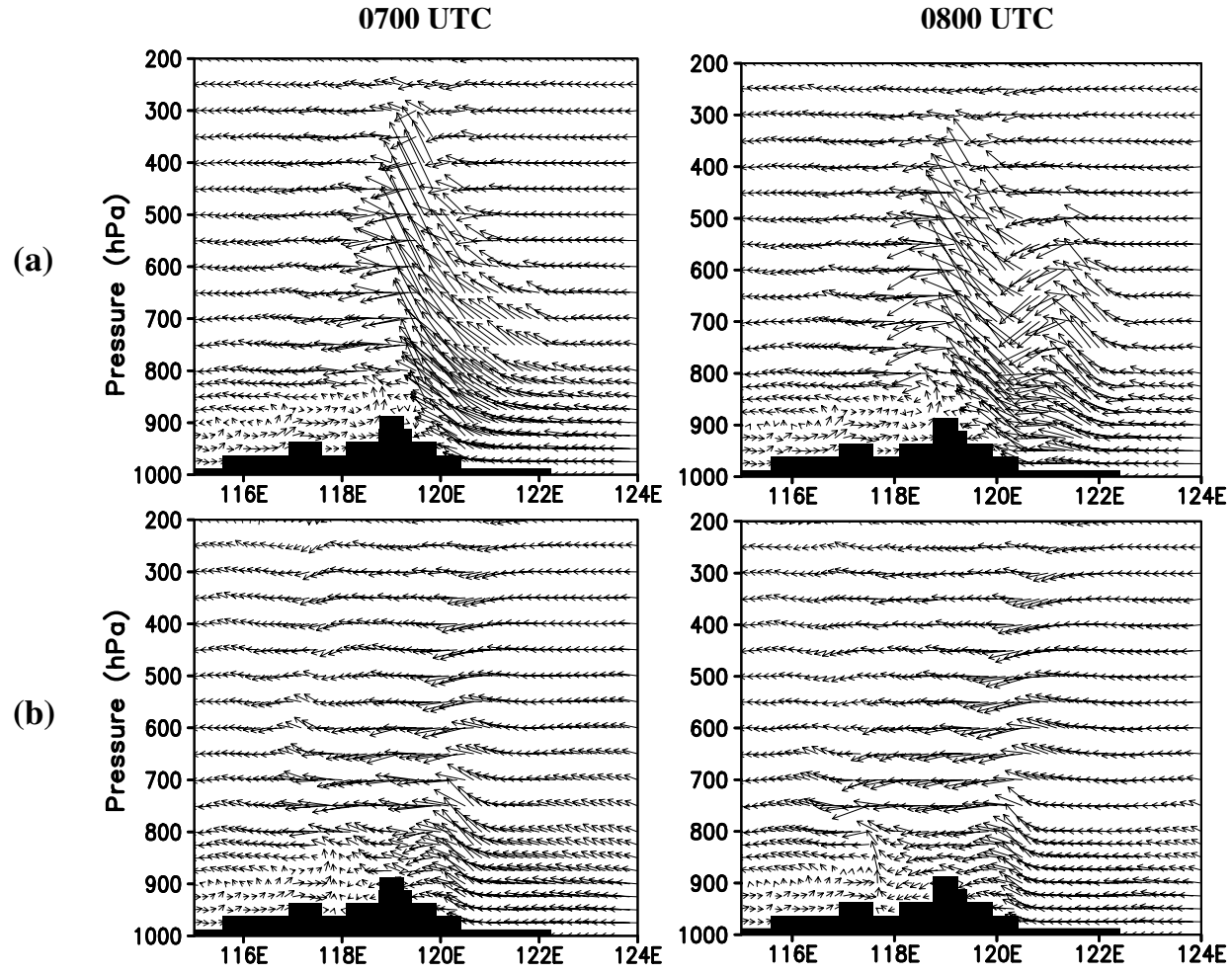

Fig. 8. Pressure-longitude cross sections of the composite vectors of zonal wind (m s^{-1}) and vertical velocity (5×10^2 m s^{-1}) along 27.5°N at 0700 UTC and 0800 UTC 25 August simulated by (a) EXP_CTL and (b) EXP_noheat.

stributions and flatter tops, demonstrating the features of stratiform rain. The results show that another possible role of LHR is to organize the convection, making the rain more centralized and stronger.

Though the total and hourly rainfall is larger when considering LHR (see Fig. 1 and Fig. 2), we find that the rainfall on the west side of the Wufeng mountain peak (WSWM) in EXP_CTL is smaller than that in EXP_noheat (see Fig. 7), which could be explained by Fig. 8. Figures 8a and b are the vertical distributions of the composite vectors of zonal wind and vertical velocity simulated by EXP_CTL and EXP_noheat, respectively. In EXP_CTL, the vertical velocity is much stronger in the ESWM, but the easterly component is relatively smaller, and the westerlies control the WSWM at 0700 and 0800 UTC. However, the wind direction is completely different in EXP_noheat. Although the westerlies dominate the WSWM below 800 hPa at 0700 UTC, they are replaced by easterlies at 0800 UTC; note that the easterlies have climbed over the Wufeng mountain peak. When the transmountain flows encounter the terrain step again, they rise and form precipitation once more, leading to a relatively larger rain area in the WSWM. Figure 8 also confirms that one possible role of the latent heat is to make the convection more organized, producing more concentrated and stronger precipitation in the ESWM and reducing the rainfall in the WSWM at the same time.

5. Conclusions and discussions

Based upon the sensitivity experiments, the southeastern China mesoscale orographic effect is examined, the role of LHR is studied and the interaction between LHR and the precipitation under the mesoscale terrain forcing is analyzed. The main conclusions are as fol-

lows:

(1) The total rain amount on 25 August 2004 produced by the typhoon Aere is tripled by mesoscale terrain in southeastern China.

(2) LHR plays a key role in the precipitation. With the condensational heating, the convection is strengthened, causing the decrease of the surface pressure. Then the pressure gradient in the E-W direction within the water vapour transport band guides the water vapour to move to the windward area of Wufeng Mountain, leading to a precipitation increase.

(3) With the LHR, the convection is more organized, producing larger vertical velocity, higher divergence height and correspondingly a smaller rain area and stronger precipitation in the ESWM. When LHR is removed from the integration, the precipitation may demonstrate stratiform rain features rather than convective rain features.

In spite of the main conclusions above, there are still some issues to be discussed:

(1) When we design sensitivity experiments to study orographic effects, especially the large-scale and higher mountains, we ought to avoid cutting the mountain height in half (or other such modifications) at the beginning of the integration, so the unbalanced initial fields may trigger some noise and interfere with the results. However, we do so. The Wufeng mountain peak is not higher than 1200 m. Compared with the deep typhoon system and the largescale rain belt, it is relatively small. The experiment also shows that if the mountain height is set to zero in the initial fields, like what we do in this paper, the unbalanced fields can basically be adjusted in two hours. Nevertheless, we do not consider the unimaginable impacts on the results.

(2) LHR is removed from the 4th to 10th hour in the sensitivity experiment. If it is removed from the beginning of the integration, the total rain amount is much smaller, and the hourly rain peak is even smaller than that in EXP_noterrain. We also tried removing LHR in the second and third hour of the integration, and we found that the earlier LHR is removed, the smaller the rainfall is. It seems that the condensational heating accumulated in the early period may affect the later precipitation.

(3) Grid scale LHR and convective LHR are not studied separately in this paper because of the relatively small convective rainfall in the AREM model. If the model horizontal resolution is improved and nonhydrostatic equilibrium is used, the extent to which LHR can increase the typhoon rainfall should be further studied.

(4) When the LHR is removed from the integration, the intensity of the typhoon system is weak and its track also shows a little change. Nevertheless, this should not impact our basic conclusions.

Acknowledgements. We thank Professor Zhou Xiaoping and two anonymous reviewers for some constructive suggestions and Professor Fu Yunfei for providing the TRMM PR data. This work was jointly supported by the National Key Basic Research and Development Project of China under Grant No. 2004CB418304 and the National Natural Science Foundation of China under Grant Nos. 40505016，40575030 and 40233031.

REFERENCES

Benjamin, S. O., and N. L. Seaman, 1985: A simple scheme for objective analysis in curved flow. *Mon. Wea. Rev.*, **113**, 1184–1198.

Betts, A. K., 1986: A new convective adjustment scheme, Part I: Observational and theoretical basis. *Quart. J. Roy. Meteor. Soc.*, **112**, 677–691.

Brennan, M. J., and G. M. Lackmann, 2005: The influence of incipient latent heat release on the precipitation distribution of the 24–25 January 2000 U.S. east coast cyclone. *Mon. Wea. Rev.*, **133**, 1913–1937.

Buzzi, A., N. Tartaglione, and P. Malguzzi, 1998: Numerical simulations of the 1994 Piedmont flood: Role of topography and moist processes. *Mon. Wea. Rev.*, **126**, 2369–2383.

Carbone, R. E., W. A. Cooper, and W. C. Lee, 1995: On the forcing of flow reversal along the windward slopes of Hawaii. *Mon. Wea. Rev.*, **123**, 34–56.

Deardorff, J. W., 1972: Parameterization of the planetary boundary layer for use in general circulation models. *Mon. Wea. Rev.*, **100**, 93–106.

Feng Qiang, Ye Rujie, Wang Angsheng, Tao Shiyan, Xu Huanbin, and Gao Shouting, 2004: The study on effects of meso-scale terrain on precipitation of torrential rain by numerical modeling. *Chinese Journal of Agrometeorology*, **25**, 1–4. (in Chinese)

Fosdick, E. K. and P. J. Smith, 1991: Latent heat release in an extratropical cyclone that developed explosively over the southeastern United States. *Mon. Wea. Rev.*, **119**, 193–207.

Gao Kun, Zhai Guoqing, Yu Zhangxiao and Tu Caihong, 1994: The simulation study of the meso-scale orographic effects on heavy rain in East China. *Acta Meteorologica Sinica*, **52**, 157–164. (in Chinese)

Holtslag, A. A. M., and B. A. Boville, 1993: Local versus nonlocal boundary-layer diffusion in a global climate model. *J. Climate*, **6**, 1825–1842.

Kodama, K. R, and G. M. Barnes, 1997: Heavy rain events over the south-facing slopes of Hawaii: Attendant conditions. *Wea. Forecasting*, **12**, 347–36.

Liu, Y. M., G. X. Wu, H. Liu., and P. Liu, 2001: Condensation heating of the Asian summer monsoon and the subtropical anticyclone in the eastern hemisphere. *Climate Dyn.*, **17**, 327–338.

Neiman, P. J., F. M. Ralph, A. B. White, D. E. Kingsmill,

and P. O. G. Persson, 2002: The statistical relationship between upslope flow and rainfall in California's coastal mountains: Observations during CALJET. *Mon. Wea. Rev.*, **130**, 1468–1492.

Pauley, P. M., and P. J. Smith, 1988: Direct and indirect effects of latent heat release on a synoptic-scale wave system. *Mon. Wea. Rev.*, **116**, 1209–1235.

Posselt, D. J., and J. E. Martin, 2004: The effect of latent heat release on the evolution of a warm occluded thermal structure. *Mon. Wea. Rev.*, **132**, 578–599.

Smith, R. B., 1979: The influence of mountains on the atmosphere. *Advances in Geophysics*, **21**, 87–137.

Tao Shiyan, 1980: *Rain Storms in China*. Science Press, Beijing, 225pp. (in Chinese)

Xu Youping, Xia Daqing, and Qian Yueying, 1998: The water-bearing numerical model and its operational forecasting experiments Part II: The operational forecasting experiments. *Adv. Atmos. Sci.*, **15**, 321–336.

Yu Rucong, 1994: Two-step shape-preserving advection scheme. *Adv. Atmos. Sci.*, **11**, 479–490.

Yu Rucong, and Xu Youping, 2004: AREM and its simulations on the daily rainfall in summer in 2003. *Acta Meteorologica Sinica*, **62**, 715–724. (in Chinese)

Zang Zengliang, Zhang Ming, Shen Hongwei, and Yao Haohai, 2004: Experiments on the sensitivity of meso-scale terrains in JangHuai area to a heavy mold rain. *Scientia Meteorologica Sinica*, **24**, 26–34. (in Chinese)

Zhai Guoqing, Gao Kun, Yu Zhangxiao, and Tu Caihong, 1995: Numerical simulation of the effects of meso-scale topography in a heavy rain process. *Scientia Atmospherica Sinica*, **19**, 475–480. (in Chinese)

Zhou Tianjun, and Qian Yongfu, 1996: An experimental study on the effects of topography on numerical prediction. *Scientia Atmospherica Sinica*, **20**, 452–462. (in Chinese)